Development of a linear brushless DC motor drive with robust position control

C.M.Liaw, R.Y.Shue, H.C.Chen and S.C.Chen

Abstract: The design and implementation of a linear brushless DC motor (LBDCM) drive with robust position control are presented. Hall-effect sensors and linear encoders are employed to obtain information of moving member position. A simple but practical zeroing approach is proposed to correct the phase errors of current commands due to the mechanical installation misalignment of Hall-effect sensors. Then a current-controlled PWM inverter is properly designed to yield excellent armature current tracking control characteristics. As to position control, the dynamic model of the LBDCM drive is first estimated from measurements. Then a two-degrees-of-freedom controller is quantitatively designed to meet the given position-control specifications. A robust controller is designed to reduce the control performance degradation due to system parameter changes and the effect of cogging force. Simulated and measured results are provided to demonstrate the driving performance of the whole linear motor drive.

1 Introduction

Compared with rotary motors, linear motors possess many advantages in linear motion driving applications, such as direct driving, low frictional loss, high position control accuracy, high speed, high acceleration and deceleration capability, large structural flexibility, high reliability etc. [1, 2]. The linear brushless DC motor (LBDCM) is basically a permanent-magnet linear synchronous motor with moving-member position sensing. Owing to its advantages such as high power density, high force–mass ratio and ease of control it has been widely employed in factory and office automation equipment [1]. However, its driving performance is highly dependent on system parameter and load variations. Many attempts have been made to improve the performance of LBDCM drives, for example, dynamic modelling [1–4], power electronics switching control [5, 6] and advanced dynamic control [5–11]. However, there are still some key issues worthy of further improvement. These include accurate position sensing, current switching control, accurate dynamic modelling, quantitative position controller design and robust control.

The key technologies toward yielding a PC-based LBDCM drive with quantitative and robust position control are presented. First, an experimental LBDCM driving one-dimensional table with Hall-effect plus an incremental encoder position-sensing scheme is established. A simple Hall-effect sensor position-zeroing approach is proposed to yield current commands that are accurately synchronised to the back-EMFs. And a current-controlled pulse-width modulated (PWM) inverter with close current command tracking characteristics is designed. Then the dynamic model of the motor drive is found by estimation from measurement. Based on the estimated model at a nominal case and the prescribed drive specifications, a two-degrees-of-freedom controller (2DOFC) [12] is quantitatively designed. Finally, for reducing the effects of cogging force, system parameter and load variations on the desired position-control performance, a robust controller is designed. Driving performance of the designed LBDCM drive is demonstrated by simulated and measured results.

IEE Proceedings online no. 20010261

DOI: 10.1049/ip-epa:20010261

Paper first received 14th June and in revised form 12th December 2000

C.M. Law, R.Y. Shue and H.C. Chen are with the Department of Electrical Engineering, National Tsing Hua University, Hschinchu, Taiwan, Republic of China

S.C. Chen is with the Chung-Shan Institute of Science & Technology, Lung-Tan, Tao-Yuan, Taiwan, Republic of China

2 LBDCM drive and dynamic modelling

2.1 System configuration

The system configuration of an experimental LBDCM drive is shown in Fig. 1, consisting of a position control loop, a speed control loop, a sinusoidal current command generator, a current loop, a current-controlled PWM inverter and an LBDCM. The LBDCM is shorted primary and has a rated continuous force of 89 N and peak force of 267 N. The current-controlled PWM inverter regulates the primary winding currents to closely follow sinusoidal commands. The constant-frequency current-controlled PWM or ramp-comparison PWM is adopted. The position control loop, velocity control loop and current command generators are realised using C-language in a PC-based control computer.

The purpose of the sinusoidal current command generator is to generate three-phase current commands with their amplitude determined by the speed control loop and their argument synchronised to the moving-member position. An incremental linear encoder with a resolution of 1.6μm per count (both A and B phases) and three Hall-effect sensors are employed to obtain the position information of the moving member. Through count multiplication the resolution of the encoder is physically increased by four times, i.e. 0.4μm per count. The purpose of the Hall-effect sensors is to check and find the exact electrical position of the motor moving member. Ideally, if the Hall-effect signals are synchronised to the back-EMFs, the correct current commands can be generated to let the primary

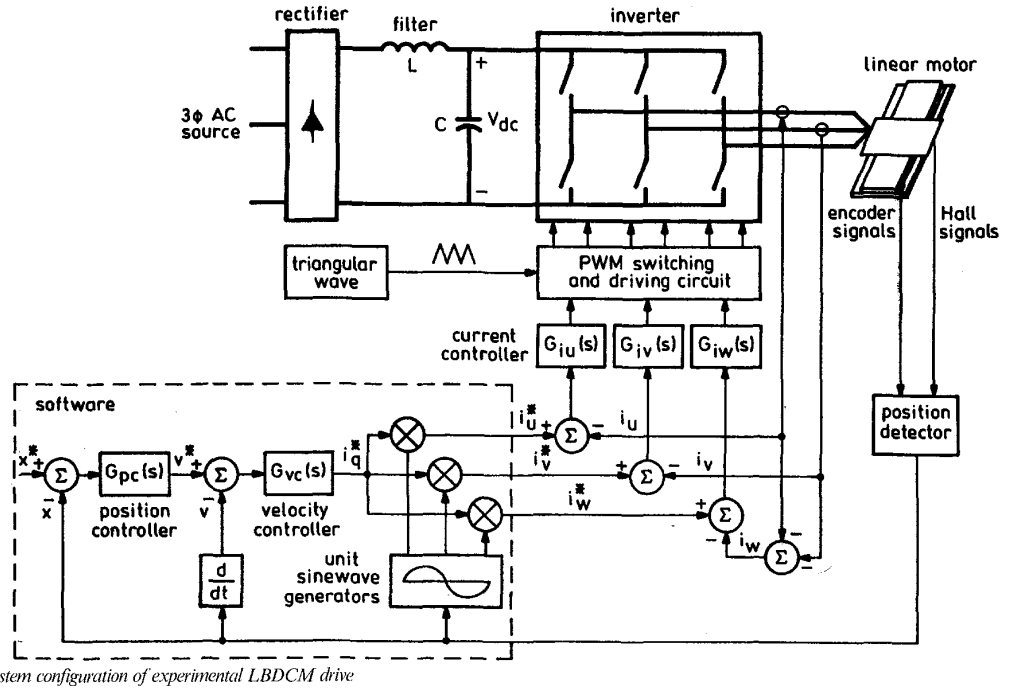

Fig. 1 *System configuration of experimental LBDCM drive*

moving-magnetic field be kept perpendicular to the secondary magnetic flux. However, this sometimes cannot be achieved perfectly, since misalignment of Hall-effect sensors due to mechanical installation may occur.

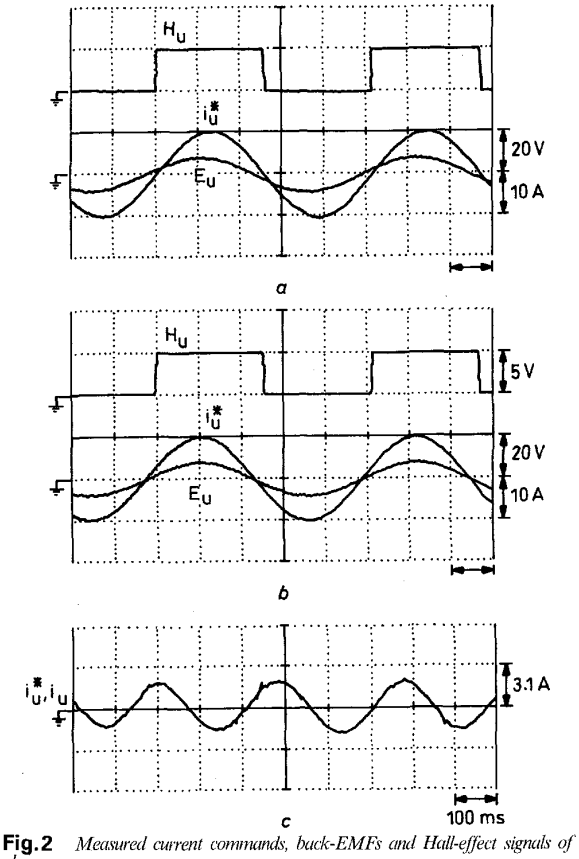

Fig. 2 *Measured current commands, back-EMFs and Hall-effect signals of phase u*
a Before making zeroing adjustment
b After making zeroing adjustment
c Measured motor current and its command

A simple zeroing technique is proposed to correct the phase errors of the sinusoidal current commands due to mechanical misalignment of Hall-effect sensors. The primary terminals are disconnected from the inverter and connected to a Y-connected resistive network for extracting the phase back-EMFs at no load. An external force is applied to let the primary move in a positive or negative direction. The measured Hall-effect signals and the back-EMFs of all phases are compared and the phase differences between them are used together with the Hall-effect signals and linear encoder position signal to make the zeroing adjustment and generate the current commands. The measured current commands, back-EMFs and the Hall-effect signals of phase u before and after making the zeroing adjustment are shown in Figs. 2*a* and *b* for positive velocity ($i_q^* = 10.0$A). One can clearly observe from Fig. 2*b* that the current commands have been kept in synchronisation with the back-EMFs. In addition, the measured motor current of phase u and its command plotted in Fig. 2*c* shows the close current-tracking control characteristics.

2.2 Model estimation

The dynamic model of a plant to be controlled is indispensable for controller analysis and design. According to the physical dynamic modelling derived in the Appendix (Section 8) the electromagnetic force equation of the LBDCM drive can be expressed as

$$F_x = K_t i_q = M\frac{d^2x}{dt^2} + B\frac{dx}{dt} + F_L + F_c \qquad (1)$$

where i_q denotes the force current component, which can be considered as $i_q \simeq i_q^*$ for the close current-tracking characteristics. Accordingly, the small-signal dynamic behaviour of the LBDCM drive shown in Fig. 1 can be represented by the control system block diagram drawn in Fig. 3*a*, wherein, for the convenience of derivation, the parameters of the motor drive plant $H_p(s)$ are defined as

$$H_p(s) = \frac{b}{s+a} \qquad (2)$$

where $a \triangleq B/M$ and $b \triangleq 1/M$. Although the dynamic model

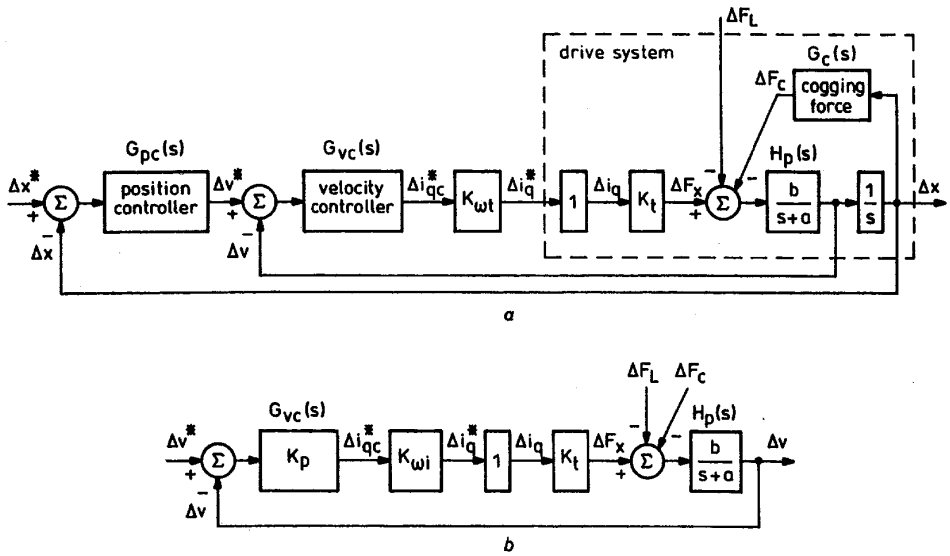

Fig. 3 *Control system block diagram*
a LBDCM drive of Fig. 1
b Velocity control loop with $G_{vc}(s) = K_p$

can be found by physical derivation described in the Appendix (Section 8), the accurate model is difficult to derive, since the accurate motor parameters are not easy to obtain. To solve this problem estimation methods [13] can be employed as an alternative to find the motor drive dynamic model from measurements.

By letting the position loop of the drive system be open and the velocity controller be a proportional type with $G_{vc}(s) = K_p = 20$, the block diagram shown in Fig. 3*a* is reduced to that shown is Fig. 3*b*. The transfer function from Δv^* to Δv can be derived from Fig. 3*b* to be

$$H_{vc}(s) \triangleq \left.\frac{\Delta v(s)}{\Delta v^*(s)}\right|_{\substack{\Delta F_L=0\\ \Delta F_c=0}} = \frac{K_p K_t' b}{s + a + K_p K_t' b} \qquad (3)$$

where $K_t' \triangleq K_{wi} K_t$ and the scaling factor $K_{wi} = 1/1.6 = 0.625$ is set here. The simplest way to identify $H_{vc}(s)$ is the step response method. However, if the proper facilities are available, the stochastic approach can be used to obtain a more accurate estimated model. A random signal with frequency range from 1 to 100Hz is applied as the speed command. After the command and measured speed input to the control system analyser (HP 3563A), the amplitude–frequency response is plotted in Fig. 4*a*. From Fig. 4*a* a first-order transfer function model is directly estimated by the curve-fitting method, which exists in the HP 3563A,

$$\hat{H}_{vc}(s) = \frac{57.282}{s + 80.754} \qquad (4)$$

The amplitude–frequency response calculated from eqn. 4 is shown in Fig. 4*b*. The result shows that it is very close to that plotted in Fig. 4*a*. From eqns. 3 and 4 one can find

$$a = 23.472 \qquad K_t' b = 2.8641 \qquad (5)$$

The transfer function from the load change ΔF_L to current change Δi_{qc}^* can be derived from Fig. 3*a* as

$$\hat{H}_{di}(s) \triangleq \left.\frac{\Delta i_{qc}^*(s)}{\Delta F_L(s)}\right|_{\substack{\Delta x^*=0\\ \Delta F_c=0}} = \frac{bG_{vc}s + bG_{pc}G_{vc}}{s^2 + (a + bG_{vc}K_t')s + bG_{pc}G_{vc}K_t'} \qquad (6)$$

From the transfer ratio at steady state the parameter K_t'

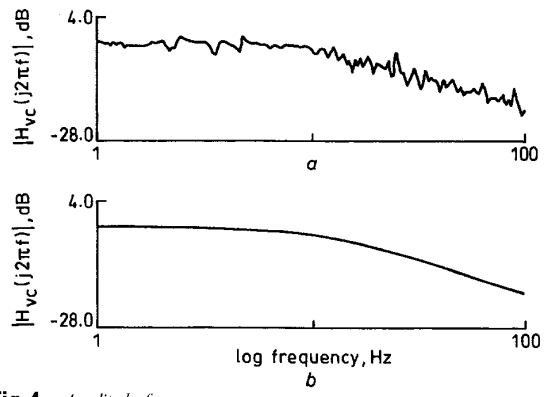

Fig. 4 *Amplitude–frequency response*
a Measured; *b* Estimated

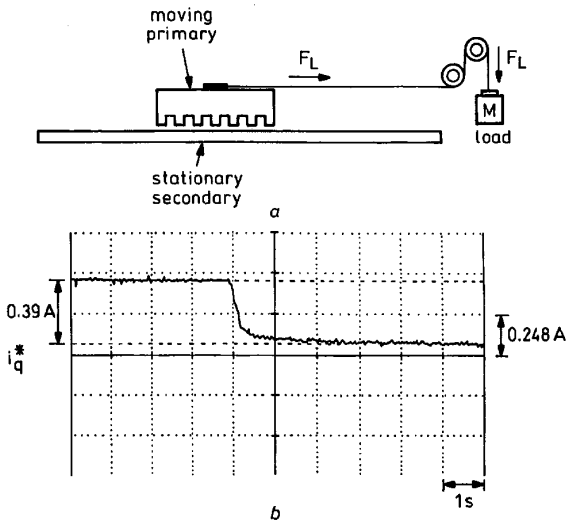

Fig. 5 *Mechanism used to estimate the force-generating constant K_t and the measured i_q^* due to a step load change of 18.081 N*

can be estimated to be

$$K_t' = \left.\frac{1}{\hat{H}_{di}(s)}\right|_{s=0} \qquad (7)$$

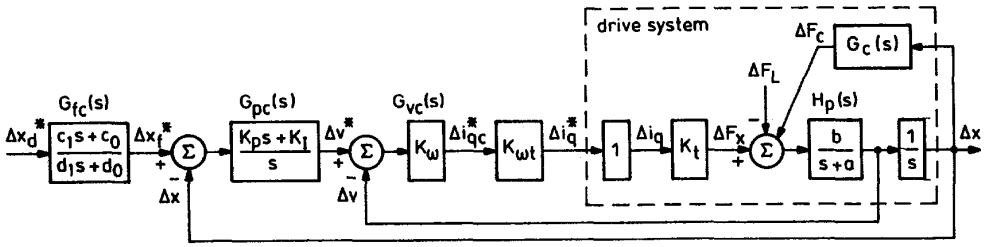

Fig. 6 *Configuration of 2DOF position controller*

A simple mechanism for making the force regulation measurement is shown in Fig. 5*a*. The response of Δi_q^* due to the step load force change is plotted in Fig. 5*b*. From the steady-state value shown in Fig. 5*b*, one can estimate $K_t' = 28.98$. Finally, all model parameters can be found from eqn. 5 as

$$a = 23.47 \qquad b = 0.0988 \qquad K_t' = 28.98 \tag{8}$$

3 2DOF position controller

To let the LBDCM servo drive possess good dynamic responses both in command tracking and load regulation, the control structure should have two degrees of freedom. The 2DOF position controller shown in Fig. 6 is employed to achieve this goal, and its design is made according to the design approach presented in [12]. The structures of the controllers $G_{vc}(s)$, $G_{pc}(s)$ and $G_{fc}(s)$ in Fig. 6 are chosen to be

$$G_{vc}(s) = K_\omega \qquad G_{pc}(s) = \frac{K_p s + K_I}{s}$$
$$G_{fc}(s) = \frac{c_1 s + c_0}{d_1 s + d_0} \tag{9}$$

In the design of 2DOFC the cogging force is neglected and its effect will be automatically compensated by the 2DOFC and the robust controller introduced in the following Section. The closed-loop tracking transfer functions of the system shown in Fig. 6 with and without the feedforward controller $G_{fc}(s)$ can be found as

$$H_{dx}^*(s) \triangleq \left.\frac{\Delta x(s)}{\Delta x_f^*(s)}\right|_{\Delta F_L(s)=0}$$
$$= \frac{bK_pK_\omega K_t' s + bK_IK_\omega K_t'}{s^3 + (a + bK_\omega K_t')s^2 + bK_pK_\omega K_t' s + bK_IK_\omega K_t'} \tag{10}$$

and

$$H_{dx}(s) \triangleq \left.\frac{\Delta x(s)}{\Delta x_d^*(s)}\right|_{\Delta F_L(s)=0}$$
$$= H_{dx}^*(s)G_{fc}(s) = H_{dx}^*(s)\frac{c_1 s + c_0}{d_1 s + d_0} \tag{11}$$

And the transfer function from the load change ΔF_L to the position change Δx can be derived as

$$H_{dd}(s) \triangleq \left.\frac{\Delta x(s)}{\Delta F_L(s)}\right|_{\Delta x_f^*(s)=0}$$
$$= \frac{-bs}{s^3 + (a + bK_\omega K_t')s^2 + bK_pK_\omega K_t' s + bK_IK_\omega K_t'}$$
$$\triangleq \left[\frac{\beta_1}{s+\mu_1} + \frac{\beta_2}{s+\mu_2} + \frac{\beta_3}{s+\mu_3}\right] \tag{12}$$

where

$$\mu_1\mu_2\mu_3 = bK_IK_\omega K_t' \tag{13}$$

$$\mu_1\mu_2 + \mu_2\mu_3 + \mu_3\mu_1 = bK_pK_\omega K_t' \tag{14}$$

$$\mu_1 + \mu_2 + \mu_3 = a + bK_\omega K_t' \tag{15}$$

$$\beta_1 + \beta_2 + \beta_3 = 0 \tag{16}$$

$$\beta_1(\mu_2 + \mu_3) + \beta_2(\mu_1 + \mu_3) + \beta_3(\mu_1 + \mu_2) = 0 \tag{17}$$

$$\beta_1\mu_2\mu_3 + \beta_2\mu_1\mu_3 + \beta_3\mu_1\mu_2 = -b \tag{18}$$

$$\beta_1 = \frac{-b}{(\mu_2-\mu_1)(\mu_3-\mu_1)} \qquad \beta_2 = \frac{-b}{(\mu_1-\mu_2)(\mu_3-\mu_2)}$$
$$\beta_3 = \frac{-b}{(\mu_1-\mu_3)(\mu_2-\mu_3)} \tag{19}$$

Although good regulation performance in eqn. 12 can be achieved by properly selecting the controller parameters K_p and K_I, satisfactory tracking performance of eqn. 10 may not be obtained simultaneously. To solve this problem a feedforward controller $G_{fc}(s)$ is added. In the design philosophy the denominator of $G_{fc}(s)$ is designed to cancel the numerator of $H_{dx}^*(s)$, and the numerator of $G_{fc}(s)$ is chosen such that good tracking characteristics will be obtained. Accordingly, $G_{fc}(s)$ and $H_{dx}(s)$ have the following forms:

$$G_{fc}(s) = \frac{c_1 s + c_0}{bK_pK_\omega K_t' s + bK_IK_\omega K_t'} \tag{20}$$

$$H_{dx}(s) = \frac{c_1 s + c_0}{s^3 + (a + bK_\omega K_t')s^2 + bK_pK_\omega K_t' s + bK_IK_\omega K_t'}$$
$$\triangleq \frac{h_1}{s+\mu_1} + \frac{h_2}{s+\mu_2} + \frac{h_3}{s+\mu_3} \tag{21}$$

with

$$h_1 + h_2 + h_3 = 0 \tag{22}$$

$$c_0 = h_1\mu_2\mu_3 + h_2\mu_1\mu_3 + h_3\mu_1\mu_2 = bK_IK_\omega K_t' \tag{23}$$

$$c_1 = h_1(\mu_2 + \mu_3) + h_2(\mu_1 + \mu_3) + h_3(\mu_1 + \mu_2) \tag{24}$$

$$d_0 = bK_IK_\omega K_t' \tag{25}$$

$$d_1 = bK_pK_\omega K_t' \tag{26}$$

Generally, a high-performance position servo drive system should possess good tracking and regulation position responses. As a result the following control specifications are defined:

- Steady-state errors both in step command tracking and load regulation responses are zero.
- Response time of tracking unit-step response defined as the time interval that the response rises from zero to 90% of its final value is t_{re}.
- Overshoot of tracking step response is zero.
- Maximum position dip due to step load force change

$$(1\,\mathrm{N}) = x_{dm} \tag{27}$$

According to the detailed derivation presented in [12], one can formulate the following nonlinear equations which incorporate the foregoing control specifications:

$$f_1(\mu_1,\mu_2,\mu_3,h_1,h_2,h_3,t_m)=\frac{h_1}{\mu_1}+\frac{h_2}{\mu_2}+\frac{h_3}{\mu_3}-1=0 \tag{28}$$

$$f_2(\mu_1,\mu_2,\mu_3,h_1,h_2,h_3,t_m)= 0.9-\left|\frac{h_1}{\mu_1}(1-e^{-\mu_1 t_{rc}})+\frac{h_2}{\mu_2}(1-e^{-\mu_2 t_{rc}}) +\frac{h_3}{\mu_3}(1-e^{-\mu_3 t_{rc}})\right|=0 \tag{29}$$

$$f_3(\mu_1,\mu_2,\mu_3,h_1,h_2,h_3,t_m)=e_2-K_1e_3=0 \tag{30}$$

$$f_4(\mu_1,\mu_2,\mu_3,h_1,h_2,h_3,t_m)=e_1-K_2(e_2+e_3)=0 \tag{31}$$

$$f_5(\mu_1,\mu_2,\mu_3,h_1,h_2,h_3,t_m)= \mu_1\beta_1e^{-\mu_1 t_m}+\mu_2\beta_2e^{-\mu_2 t_m}+\mu_3\beta_3e^{-\mu_3 t_m}=0 \tag{32}$$

$$f_6(\mu_1,\mu_2,\mu_3,h_1,h_2,h_3,t_m)= \Delta x_{dm}-\beta_1e^{-\mu_1 t_m}-\beta_2e^{-\mu_2 t_m}-\beta_3e^{-\mu_3 t_m}=0 \tag{33}$$

where $\mu_1 < \mu_2 < \mu_3$, $K_1 > 0$ and $K_2 < -1$. The unknown parameters in eqns. 28–33 are μ_1, μ_2, μ_3, h_1, h_2 and t_m. To satisfy the condition of $\mu_1 < \mu_2 < \mu_3$ the parameters μ_2 and μ_3 are further modified to

$$\mu_2=\mu_1+c_2^2 \qquad \mu_3=\mu_1+c_2^2+c_3^2 \tag{34}$$

where c_2^2 and c_3^2 are positive and finite. Thus the unknown parameters in the nonlinear equations eqns. 28–33 become μ_1, c_2, c_3, h_1, h_2 and t_m. These unknown parameters can be solved by Matlab programs. Then the parameters of the controllers $G_{vc}(s)$ and $G_{pc}(s)$ can be found using the relationship of eqns. 13–15 as follows:

$$K_\omega=(\mu_1+\mu_2+\mu_3-a)/(bK_t') \tag{35}$$

$$K_p=(\mu_1\mu_2+\mu_2\mu_3+\mu_1\mu_3)/(bK_\omega K_t') \tag{36}$$

$$K_I=(\mu_1\mu_2\mu_3)/(bK_\omega K_t') \tag{37}$$

and the parameters of the $G_{fc}(s)$ controller can be found from the relationships of eqns. 23–26.

3.1 Numerical design

The dynamic model of the LBDCM drive has been estimated previously and given in eqn. 8. The control specifications are given eqn. 27 with t_{re} = 0.1s and $\Delta x_{dm} = 2 \times 10^{-5}$m due to ΔF_L = 1 N. Letting K_1 = 1 and K_2 = –2 and following the aforementioned design procedure, the parameters of the controllers $G_{vc}(s)$, $G_{pc}(s)$ and $G_{fc}(s)$ can be found to be

$$G_{vc}(s)=K_\omega=30.63 \tag{38}$$

$$G_{pc}(s)=\frac{K_ps+K_I}{s}=\frac{45.84s+531.75}{s} \tag{39}$$

$$G_{fc}(s)=\frac{c_1s+c_0}{d_1s+d_0}=\frac{2094s+59481}{5128s+59481} \tag{40}$$

3.2 Simulation and experimental results

With the feedforward controller first disabled, Fig. 7*a* shows the simulated position response due to a position step command change of 0.5cm by the 1DOF controller (PI structure of $G_{pc}(s)$). After the feedforward controller $G_{fc}(s)$ is applied to form a complete 2DOFC as shown in Fig. 6 the simulated results are shown in Fig. 7*b*. Since the load regulation behaviour is not relevant to the feedforward controller $G_{fc}(s)$, the position responses due to a step load force change of 10 N by 1DOFC and 2DOFC are identical and plotted in Fig. 7*c*. The results in Figs. 7*a* to *c* show that the prescribed tracking and regulation control performance are completely satisfied by the designed 2DOFC, but the 1 DOFC fails to achieve this.

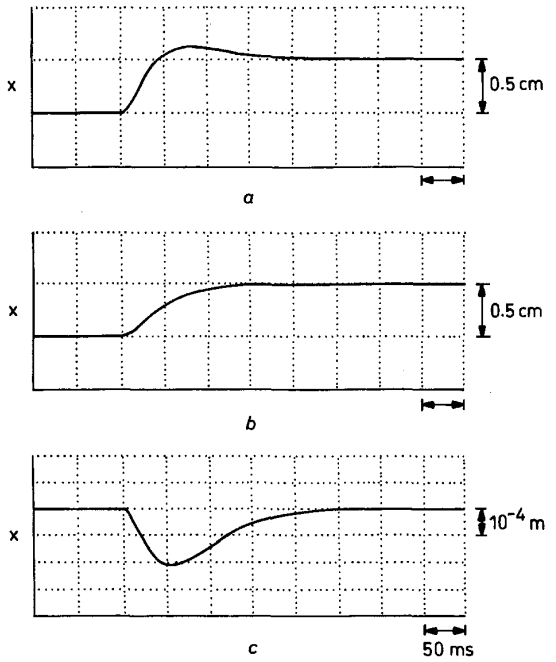

Fig. 7 *Simulated position responses*
a Due to position step command change of 0.5cm by 1DOFC
b As (*a*) by 2DOFC
c Due to step load force change of 10 N by 1DOFC and 2DOFC

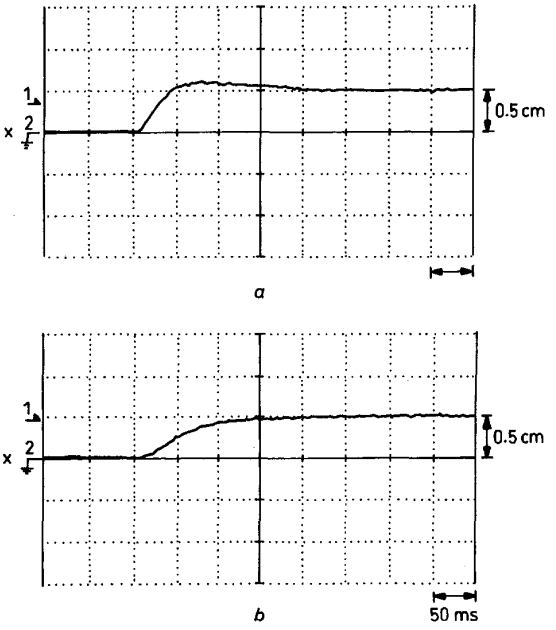

Fig. 8 *Measured position responses*
a Due to position step command change of 0.5cm by 1DOFC
b As (*a*) by 2DOFC

After confirming the validity of the designed 2DOFC, the discrete realisation of the designed control law is made. The measured results by 1DOFC and 2DOFC with the same conditions as those of Figs. 7*a* and *b* are shown in Figs. 8*a* and *b*. The same comments as those made for simulation can also be deduced from these measured tracking responses. Since the rigid load changing mechanism is not available the measured results of load regulation are not provided.

4 Robust position controller

When the load changes and operating condition variations occur the desired control performances will not be kept by the position 2DOF controller designed at nominal case. To solve this problem a position robust controller based on the concept of direct disturbance cancellation is designed. Configuration of the robust 2DOF position controller is shown in Fig. 9 [12], wherein the 2DOFC is used to fit the driving specifications specified at nominal case, and the robust controller is used to reduce the effects of load change and parameter variations. The weighting factor W is used to set the extent of disturbance cancellation. At the nominal case, the contribution of the robust controller is zero, i.e. $\Delta i_{qr}^* = 0$. When load or system parameter changes occur a control signal Δi_{qr}^* will be automatically generated to compensate for these effects.

Suppose that the mass M and the damping ratio B of the moving member deviate from their nominal values $\bar{M}$ and $\bar{B}$ to

$$M \triangleq \bar{M} + \Delta M \qquad B \triangleq \bar{B} + \Delta B \tag{41}$$

and the force constant is relatively constant, i.e. $\bar{K}_t = \bar{K}_t'$. One can derive the following relationship from Fig. 9:

$$\begin{aligned} K_t' \Delta i_{qe}^* = {} & \left(\bar{M} + (1-W)\Delta M\right)\Delta\ddot{x} \\ & + \left(\bar{B} + (1-W)\Delta B\right)\Delta\dot{x} \\ & + (1-W)\Delta F_L + (1-W)\Delta F_c \end{aligned} \tag{42}$$

From Fig. 9 and eqn. 42 one can see that the effects of the cogging force, the load force disturbance and the parameter variations have been reduced by a factor of $(1 - W)$. The larger value of W $(0 \le W \le 1)$ is chosen, the better is the control performance. However, a large control effort will lead to hard control saturation, and moreover, the system will become unstable if nonlinearities exist. As a result the weighting factor W should be properly set by considering a compromise between the desired performance and the required control effort. For the theoretical basis for strictly determining the weighting factor refer to [14, 15].

4.1 Simulation and experimental results

To test the effectiveness of the proposed robust controller a load mass is supposed to change to let the drive model change from the nominal case listed in eqn. 8 to

$$H_p(s) = \frac{0.0198}{s + 4.694} \qquad (M = 5\bar{M}) \tag{43}$$

The simulated position and current responses due to step command change for various values of weighting factors are shown in Figs. 10*a* and *b*. For comparison the responses at the nominal case are also plotted. For the

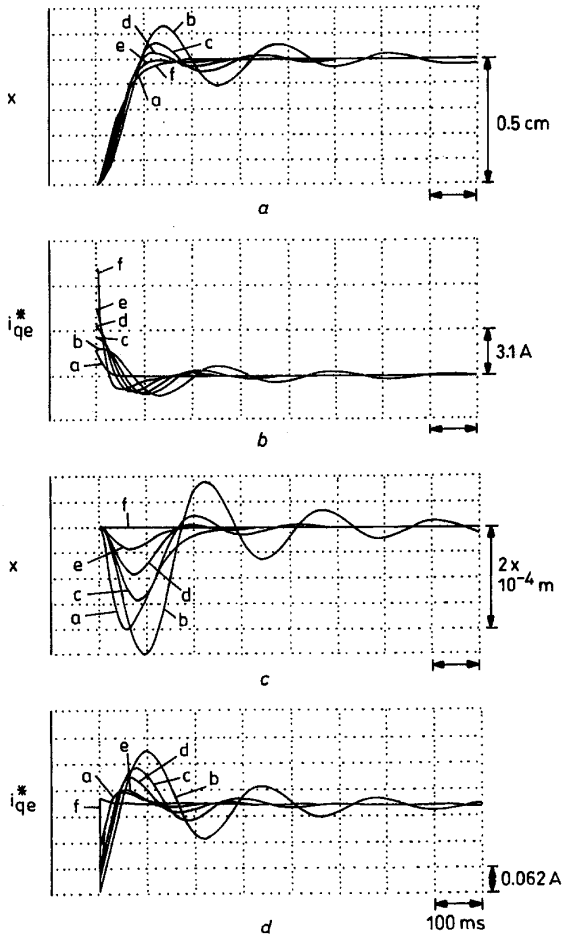

Fig. 10 *Simulated responses by robust 2DOFC with different values of W*
a Positions
b Currents due to step command change
c Positions
d Currents due to step load force change (10 N)
a $W = 0$, $M = \bar{M}$ *d* $W = 0.6$, $M = 5\bar{M}$
b $W = 0.2$, $M = 5\bar{M}$ *e* $W = 0.8$, $M = 5\bar{M}$
c $W = 0.4$, $M = 5\bar{M}$ *f* $W = 1.0$, $M = 5\bar{M}$

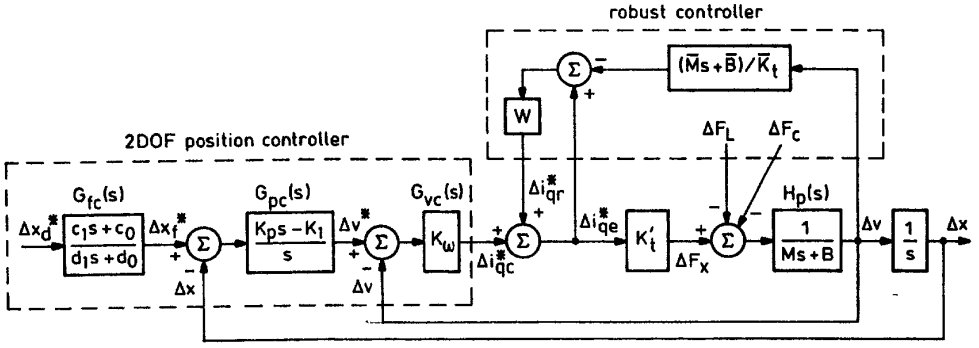

Fig. 9 *Configuration of robust 2DOF position controller*

same cases the responses of step load force regulation are shown in Figs. 10*c* and *d*. The results in Figs. 10*a* to *d* indicate that the larger value of W will lead to better performance but suffers from larger control effort.

For testing the effectiveness of the proposed controller, a load mass M_{load} = 15.7kg is added to the motor driven table. The measured position and current responses due to a step position command change (0.5cm) for three values of W are plotted in Figs. 11*a* to *c*. The measured results reveal that without the compensation by the robust controller, some overshoots and oscillations occur. By increasing the values of the weighting factor the responses are improved but the required control efforts (i.e. currents) are increased correspondingly.

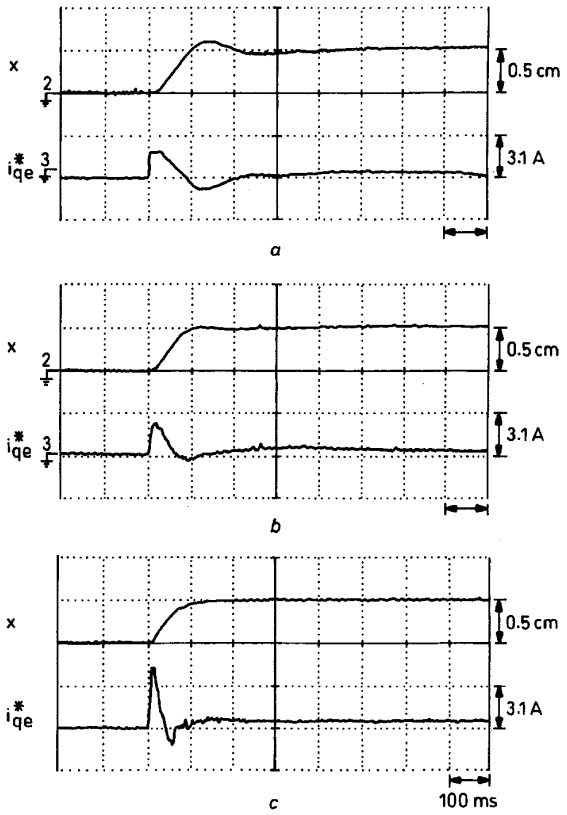

Fig. 11 *Measured position and current responses by robust 2DOFC due to step position command change (0.5cm)*
a $W = 0$
b $W = 0.4$
c $W = 1$

5 Conclusions

A linear brushless DC motor drive and its position controller have been developed. An experimental LBDCM position servo drive system was established, wherein three Hall-effect sensors and an incremental linear encoder are employed to obtain the position information of a motor moving member. A PC-based control computer is employed to realise the proposed control algorithms. It is known that excellent current response in armature windings is the key to achieving a high-performance servo drive. A current-controlled PWM voltage source inverter with low distortion sinusoidal output current was developed for powering the armature windings. In addition, a simple but practical tuning approach is proposed to let the current commands be synchronised to the back-EMFs such that better force generating capability is achieved.

As to the development of a high-performance position controller, the motor drive dynamic model is estimated from input/output measurements, and then the design equations of a 2DOF position controller formulated. Through these equations the parameters of 2DOFC were found systematically to meet the desired step position command tracking and regulation responses. As the parameter and operating condition changes occur, a robust controller is further developed and applied to preserve the prescribed control requirements. The performance of the developed LBDCM drive has been demonstrated by simulation and experimental results.

6 Acknowledgment

This research work was supported by the Ministry of Economic Affairs, Taiwan, Republic of China, under grant 88EC2A170150.

The authors wish to thank the referee for his kind comments. Revisions are made in accordance with the referees' comments.

7 References

1 EASTHAM, J.F.: 'Novel synchronous machines: linear and disc', *IEE Proc. B, Electr. Power Appl.*, 1990, **137**, (1), pp. 49–58
2 BOLDEA, I., and NASAR, S.A.: 'Linear electric actuators and generators' (Cambridge University Press, UK, 1997)
3 DENG, Z., BOLDEA, I., and NASAR, S.A.: 'Forces and parameters of permanent magnet linear synchronous machines', *IEEE Trans. Magn.*, 1987, **MAG-23**, (1), pp. 305–309
4 PILLAY, P., and KRISHNAN, R.: 'Modelling of permanent magnet motor drives', *IEEE Trans. Ind. Electron.*, 1988, **IA-35**, (4), pp. 537–541
5 HASHIMOTO, H., NAKAYAMA, T., KONDO, S., and HARASHIMA, F.: 'Variable structure approach for brushless servo motor control', *Electr. Eng. Jpn.*, 1989, **109**, (6), pp. 116–122
6 TAKAHASHI, I., and IDE, Y.: 'Decoupling control of thrust and attractive force of a LIM using a space vector control inverter', *IEEE Trans. Ind. Appl.*, 1993, **IA-29**, (1), pp. 161–167
7 UMENO, T., and HORI, Y.: 'Robust DC servo system design based on the parameterization of two degrees of freedom control system'. Proceedings of IEEE annual meeting on *Industrial electronics*, 1989, pp. 313–318
8 UMENO, T., and HORI, Y.: 'Robust speed control of DC servo motors using modern two degrees-of-freedom controller design', *IEEE Trans. Ind. Electron.*, 1991, **IE-33**, (5), pp. 363–368
9 FAMOURI, P.: 'Control of a linear permanent magnet brushless DC motor via exact linearization methods', *IEEE Trans. Energy Convers.*, 1992, **EC-7**, (3), pp. 544–551
10 EGAMI, T., and TSUCHIYA, T.: 'Disturbance suppression control with preview action of linear DC brushless motor', *IEEE Trans.*, 1993, **IE-42**, (5), pp. 494–500
11 MOGHANI, J.S., and EASTHAM, J.F.: 'The dynamic response of a linear brushless DC motor'. Proceedings of international conference on *Power electronics, drives and energy systems for industrial growth*, 1996, pp. 599–602
12 LIAW, C.M., LIN, F.J., SHIEH, Y.S., GUEY, R.J., and HWANG, M.S.: 'Robust two-degree-of-freedom control for induction motor servo drives', *IEE Proc. B, Electr. Power Appl.*, 1995, **142**, (2), pp. 79–86
13 LIAW, C.M.: 'System parameter estimation from sampled data', *Control Dyn. Syst.*, 1994, **63**, pp. 161–195
14 LIAW, C.M., and CHIANG, S.J.: 'Robust control of multimodule current model controlled converters', *IEEE Trans. Power Electron.*, 1993, **PE-8**, (4), pp. 455–465
15 LIN, F.J., and LIAW, C.M.: 'Control of indirect field-oriented induction motor drives considering the effects of dead-time and parameter variations', *IEEE Trans. Ind. Electron.*, 1993, **IE-40**, (5), pp. 486-495

8 Appendix

8.1 Dynamic model derivation

Assumptions: end-effect is neglected; magnetic system is to be linear; back-EMFs are sinusoidal; air gap is uniform; and three-phase moving member windings are symmetrical and sinusoidally distributed. The voltage equations of a P-pole LBDCM can be represented as [9]

$$\boldsymbol{v}_{abcs} = \boldsymbol{r}_s \boldsymbol{i}_{abcs} + \frac{d}{dt}\lambda_{abcs} \qquad (44)$$

$$\lambda_{abcs} = \boldsymbol{L}_s \boldsymbol{i}_{abcs} + \lambda_m \tag{45}$$

$\boldsymbol{L}_s =$

$$\begin{bmatrix} L_{ls}+L_A-L_B\cos\left(\frac{P\pi x}{\tau}\right) & -\frac{1}{2}L_A-L_B\cos\left(\frac{P\pi x}{\tau}-\frac{2\pi}{3}\right) & -\frac{1}{2}L_A-L_B\cos\left(\frac{P\pi x}{\tau}-\frac{4\pi}{3}\right) \\ -\frac{1}{2}L_A-L_B\cos\left(\frac{P\pi x}{\tau}-\frac{2\pi}{3}\right) & L_{ls}-L_A-L_B\cos\left(\frac{P\pi x}{\tau}-\frac{4\pi}{3}\right) & -\frac{1}{2}L_A-L_B\cos\left(\frac{P\pi x}{\tau}\right) \\ -\frac{1}{2}L_A-L_B\cos\left(\frac{P\pi x}{\tau}-\frac{4\pi}{3}\right) & -\frac{1}{2}L_A-L_B\cos\left(\frac{P\pi x}{\tau}\right) & L_{ls}-L_A-L_B\cos\left(\frac{P\pi x}{\tau}-\frac{2\pi}{3}\right) \end{bmatrix} \tag{46}$$

$\lambda_m =$

$$\lambda_{max}\left[\sin\left(\frac{P\pi x}{2\tau}\right) \quad \sin\left(\frac{P\pi x}{2\tau}-\frac{2\pi}{3}\right) \quad \sin\left(\frac{P\pi x}{2\tau}-\frac{4\pi}{3}\right)\right]^T \tag{47}$$

where L_A and L_B denote the defined parameters related to motor physical parameters, and

$\boldsymbol{v}_{abcs} = [v_{as}\ v_{bs}\ v_{cs}]^T$: moving-member phase voltage vector

$\boldsymbol{i}_{abcs} = [i_{as}\ i_{bs}\ i_{cs}]^T$: moving-member phase current vector

$\boldsymbol{r}_s = diag\ [r\ r\ r]^T$: resistance matrix of moving-member winding

$\lambda_{abcs} = [\lambda_{as}\ \lambda_{bs}\ \lambda_{cs}]^T$: moving-member flux linkage vector

L_{ls}: leakage inductance

x: position of moving member

P: number of poles

τ: pole pitch

λ_{max} amplitude of sinusoidal flux linkages of moving-member windings

As the currents are known the electromagnetic generating force and mechanical equations can be found

$$F_x = \frac{P}{2}\frac{dW_{abcs}}{dx} = M\frac{d^2x}{dt^2} + B\frac{dx}{dt} + F_L + F_c \tag{48}$$

with the total stored energy

$$W_{abcs} = \frac{1}{2}\left[\boldsymbol{i}_{abcs}^T(\boldsymbol{L}_s - L_{ls}I)\boldsymbol{i}_{abcs} + \boldsymbol{i}_{abcs}^T\lambda_m\right] \tag{49}$$

where $\boldsymbol{I}$ denotes the unity matrix with proper dimensions, and $M = M_{motor} + M_{load}$ = total mass of moving member, $B = B_{motor} + B_{load}$ = total damping ratio, F_L = load force and F_c = cogging force. The transformation of variables from *abc* domain to secondary frame can be written as

$$\boldsymbol{h}_{qd0s} = \boldsymbol{K}_s \boldsymbol{h}_{abcs} \tag{50}$$

with

$\boldsymbol{K}_s =$

$$\frac{2}{3}\begin{bmatrix} \cos\left(\frac{P\pi x}{2\tau}\right) & \cos\left(\frac{P\pi x}{2\tau}-\frac{2\pi}{3}\right) & \cos\left(\frac{P\pi x}{2\tau}-\frac{4\pi}{3}\right) \\ \sin\left(\frac{P\pi x}{2\tau}\right) & \sin\left(\frac{P\pi x}{2\tau}-\frac{2\pi}{3}\right) & \sin\left(\frac{P\pi x}{2\tau}-\frac{4\pi}{3}\right) \\ \frac{1}{2} & \frac{1}{2} & \frac{1}{2} \end{bmatrix} \tag{51}$$

where $\boldsymbol{h}_{qd0s} = [h_{qs}\ h_{ds}\ h_{0s}]^T$ and $\boldsymbol{h}_{abcs} = [h_{as}\ h_{bs}\ h_{cs}]_T$; h can be voltage, current or flux linkage. By using the assumptions made and through proper arranging, one can derive the following propulsion force expression for a P-pole LBDCM:

$$F_x = \frac{3}{2}\frac{P}{2}\frac{\pi}{\tau}\lambda_{max} i_q \triangleq K_t i_q \tag{52}$$

where K_t denotes the force generating constant.